Published in final edited form as:

Cancer Immunol Res. 2019 September ; 7(9): 1412–1425. doi:10.1158/2326-6066.CIR-19-0258.

Engineered adoptive T-cell therapy prolongs survival in a preclinical model of advanced stage ovarian cancer

Kristin G. Anderson[1,2], **Valentin Voillet**[3], **Breanna M. Bates**[2], **Edison Y. Chiu**[1], **Madison G. Burnett**[2], **Nicolas M. Garcia**[2], **Shannon K. Oda**[1,2], **Christopher B. Morse**[2,4], **Ingunn M. Stromnes**[1,2,5], **Charles W. Drescher**[6], **Raphael Gottardo**[3], **Philip D. Greenberg**[1,2]

[1.]Department of Immunology, University of Washington School of Medicine, Seattle, WA 98109

[2.]Clinical Research Division, Fred Hutchinson Cancer Research Center, Seattle, WA 98109, USA

[3.]Vaccine and Infectious Disease Division, Fred Hutchinson Cancer Research Center, Seattle, WA 98109

[4.]Division of Gynecologic Oncology, Department of Obstetrics and Gynecology, University of Washington, Seattle, WA 98195

[5.]Current address: Department of Microbiology and Immunology, Center for Immunology, University of Minnesota, Minneapolis, MN 55455

[6.]Translational Outcomes Research, Fred Hutchinson Cancer Research Center, Seattle, WA 98109

Abstract

Adoptive T-cell therapy using high-affinity T-cell receptors (TCRs) to target tumor antigens has potential for improving outcomes in high-grade serous ovarian cancer (HGSOC) patients. Ovarian tumors develop a hostile, multicomponent tumor microenvironment containing suppressive cells, inhibitory ligands, and soluble factors that facilitate evasion of antitumor immune responses. Developing and validating an immunocompetent mouse model of metastatic ovarian cancer that shares antigenic and immunosuppressive qualities of human disease would facilitate establishing effective T-cell therapies. We used deep transcriptome profiling and immunohistochemical analysis of human HGSOC tumors and disseminated mouse $ID8_{VEGF}$ tumors to compare immunologic features. We then evaluated the ability of CD8 T cells engineered to express a high-affinity TCR specific for mesothelin, an ovarian cancer antigen, to infiltrate advanced $ID8_{VEGF}$ murine ovarian tumors and control tumor growth. Human CD8 T cells engineered to target mesothelin were also evaluated for ability to kill HLA-$A2^+$ HGSOC lines. Immunohistochemistry and gene expression profiling revealed striking similarities between tumors of both species, including processing/presentation of a leading candidate target antigen, suppressive immune cell

Correspondence: Philip D. Greenberg, MD, Fred Hutchinson Cancer Research Center, Mail Stop D3-100, P.O. Box 19024, Seattle, WA 98109-1024, pgreen@uw.edu.

Author Contributions: Conceptualization, K.G.A. C.B.M. C.W.D., and P.D.G.; Methodology, K.G.A., V.V., R.G., and P.D.G.; Validation, V.V. and R.G.; Data Acquisition and Analysis, K.G.A., B.B., E.Y.C., M.G.B., and N.M.G.; Resources, S.O., I.M.S., C.D.; Writing – Original Draft, Review and Editing, K.G.A., V.V., B.B., R.G., P.D.G.; Funding Acquisition, K.G.A. and P.D.G; Supervision, K.G.A., R.G. and P.D.G.

Conflict of Interest statement: P.D.G. and S.K.O. have patents with and P.D.G. is a scientific consultant for Juno Therapeutics.

infiltration, and expression of molecules that inhibit T-cell function. Engineered T cells targeting mesothelin infiltrated mouse tumors but became progressively dysfunctional and failed to persist. Treatment with repeated doses of T cells maintained functional activity, significantly prolonging survival of mice harboring late-stage disease at treatment onset. Human CD8 T cells engineered to target mesothelin were tumoricidal for three HGSOC lines. Treatment with engineered T cells may have clinical applicability in patients with advanced-stage HGSOC.

Keywords

High Grade Serous Ovarian Cancer; Adoptive T-cell Immunotherapy; Immunocompetent Mouse Model

INTRODUCTION

22,000 women are diagnosed with high-grade serous ovarian cancer (HGSOC) annually in the United States (seer.cancer.gov). The current standard of care includes cytoreductive surgery and combination chemotherapy (1). Over 70% of ovarian cancer patients diagnosed with advanced disease relapse, and more than half die within 5 years of diagnosis (1), which has changed little in the last 20 years (2).

Substantial evidence suggests HGSOC is an immunogenic tumor. Tumor antigen (Ag)–reactive T cells and antibodies are detectable in patient blood and ascites (3), and tumor infiltrates of cytotoxic $CD8^+$ T-cells correlate with favorable outcomes (4). Activation of antitumor immune responses, through vaccination, IL2 administration, checkpoint blockade, or infusion of *ex vivo* expanded tumor-infiltrating lymphocytes has produced only modest responses in ovarian cancer patients (4). Thus, endogenous T cells can have antitumor activity, but therapeutic efficacy is constrained by limited immunogenic epitopes, generally low-avidity T-cell responses from patient repertoires to most of the targetable tumor-associated Ags, and the immunosuppressive tumor microenvironment (TME) that typifies HGSOC tumors (3). Engineering T cells to express high-affinity T-cell receptors (TCRs) targeting ovarian cancer Ags has the potential to create responses with the desired specificity, function, and avidity, regardless of the endogenous T-cell repertoire (5), and to address efficacy-reducing inhibitory pathways (6–8). Targeting proteins overexpressed by tumors has in some settings controlled tumor growth with little or no toxicity to healthy tissues (9–11). Studies have identified mesothelin (MSLN) as a promising tumor Ag in ovarian cancer (12): it is overexpressed in >75% of HGSOC tumors, contributes to the malignant and invasive phenotype, and has limited expression in healthy cells (13).

T cells expressing engineered chimeric antigen receptors (CARs) have shown great success against hematologic malignancies. CARs usually consist of an antibody (Ab) single-chain variable fragment, as the recognition structure, fused to a T-cell signaling molecule(s). MSLN-specific CAR-T cells are being tested in ovarian cancer (13). However, the CAR construct recognizes MSLN protein rather than a peptide:major histocompatibility complex (pMHC), such that CAR-T cells may target normal tissues expressing membrane MSLN even with limited MHC expression (14), and bind MSLN protein shed from tumor cells, reducing therapeutic activity (15). In contrast, TCRs recognize peptides presented on MHC

molecules, and tumor cells can present MSLN peptides, despite MSLN protein shedding. Thus, MSLN-specific TCR-T cells represent an adoptive immunotherapy alternative for targeting ovarian cancer.

The transplantable ID8 murine ovarian cancer cell line (16) was transduced to highly express vascular endothelial growth factor (VEGF) to mimic the elevated expression observed in many patients (17). The $ID8_{VEGF}$ murine model recapitulates human advanced-stage HGSOC, with aggressive growth, dissemination throughout the peritoneal cavity, and development of hemorrhagic ascites (17,18). However, it is not clear to what extent $ID8_{VEGF}$ tumors mimic the suppressive immune microenvironment of human disease. Our study aimed to determine if $ID8_{VEGF}$ can appropriately model human HGSOC for testing cellular immunotherapy and to identify obstacles to efficacy addressable by modulation of the immune system and tumor microenvironment in future iterative studies. Our analysis by deep transcriptome profiling and immunohistochemical (IHC) analyses revealed that advanced human HGSOC and mouse $ID8_{VEGF}$ tumors express similar molecular pathways potentially impacting the efficacy of T cell-based immunotherapies. Therefore, we assessed the therapeutic activity of administering T cells engineered to express a murine Msln-specific TCR, which we previously showed have antitumor activity without toxicity to normal tissues in a pancreas cancer model (19)). Unlike most published studies in ID8 models that begin therapy when tumor is difficult to detect (<2 weeks after tumor cell injection), we initiated treatment only after disseminated tumors were detectable in the abdomen by high-resolution ultrasound (at ~6 weeks), paralleling the disease burden commonly targeted in patients. These studies have both demonstrated the potential to achieve therapeutic benefit and identified potential obstacles to clinical efficacy that can now be systematically addressed.

MATERIALS AND METHODS

Cell lines

The Kuramochi, TYKNU, OVKATE, OVSAHO, COV318, and OAW28 human cells lines were a gift from Dr. Beth Karlan at Cedars-Sinai Medical Center. COV362 was ordered from ATCC. OVCAR3 cells were a gift from the Pacific Ovarian Cancer Research Consortium (POCRC) Repository. All human cell lines were received in 2015 and passaged fewer than 10 times before use in experiments. ID8 cells and $ID8_{VEGF}$ cells, which were transduced to overexpress vascular endothelial growth factor (VEGF) to recapitulate the elevated levels observed in human disease (14), were a gift from Dr. Matthias Stephan in 2014. All ID8 cell lines were passaged fewer than 15 times before use in experiments. All human and mouse cell lines were confirmed negative for mycoplasma prior to use. Cell lines were not authenticated in the past year.

See Supplemental Table 1 or DOI for cell culture information: dx.doi.org/10.17504/protocols.io.2h7gb9n

Mouse strains

The Institutional Animal Care and Use Committees of the University of Washington and the Fred Hutchinson Cancer Research Center approved all animal studies. 5×10^6 $ID8_{VEGF}$ (17) cells were injected i.p. into 6–7 week old female C57BL/6J mice (Jackson Laboratories). P14 mice have been previously described (20).

Human specimens

All studies using human specimens were approved by the Fred Hutchinson Cancer Research Center Institutional Review Board and conducted according to the principles expressed in the Declaration of Helsinki. Tumor tissues were obtained by the POCRC Repository from patients who provided written informed consent.

Retroviral constructs

The codon-optimized murine Vβ9 and Vα4 TCR chains, connected by a porcine teschovirus-1 2A element ("P2A"; Life technologies), recognize the $Msln_{406–414}$ epitope presented in H2-D^b, and were cloned from the Mig-R1 retroviral vector (19) into the pENTR vector and subsequently Gateway cloned into the pMP71 retroviral vector for all TCR_{1045} studies. The codon-optimized murine Vβ5 and Vα2 TCR chains, also linked by a P2A element (Life technologies), bind an ovalbumin epitope ($OVA_{257–264}$, "SIINFEKL") presented in H2-K^d, and were cloned into the pENTR vector and Gateway cloned into the pMP71 retroviral vector.

See Supplemental Table 2 for $Msln_{406–414}$ TCR_{1045} and $\underline{TCR}_{OTI}$ sequences.

TCR transduction of T cells

See DOI for murine T-cell transduction: dx.doi.org/10.17504/protocols.io.smrec56

See DOI for murine T-cell re-stimulation: dx.doi.org/10.17504/protocols.io.spqedmw

See DOI for human T-cell transduction and Rapid Expansion Protocol: dx.doi.org/10.17504/protocols.io.sxvefn6

Adoptive immunotherapy

$ID8_{VEGF}$-tumor-bearing mice received either engineered T cells (1×10^7, transduced and re-stimulated *in vitro*) or engineered T cells (1×10^7) transduced without restimulation *in vitro* but then stimulated *in vivo* with 5×10^7 peptide-pulsed irradiated splenocytes as a vaccine. Cell infusions were followed by IL2 (2×10^4 IU, s.c.) daily for 10 days to promote T-cell expansion and survival. For therapy with serial T-cell infusions, mice received this same treatment protocol every 2 weeks. In indicated experiments, treated mice received one dose of Cyclophosphamide (180 mg/kg) i.p. to lymphodeplete hosts approximately 6–8 hours prior to only the first T-cell infusion.

Histology and immunohistochemistry (IHC)

See DOI for IHC: dx.doi.org/10.17504/protocols.io.sppedmn

See Supplemental Table 3 or DOI for primary and secondary antibody information and antigen retrieval method for murine IHC: dx.doi.org/10.17504/protocols.io.2h8gb9w

See Supplemental Table 4 or DOI for primary and secondary antibody information and antigen retrieval method for human IHC: dx.doi.org/10.17504/protocols.io.2ibgcan

Isolation of mononuclear cells from tissues

See DOI for T-cell isolation: dx.doi.org/10.17504/protocols.io.sqnedve

Flow cytometry

$MSLN_{406–414}$/H2-D^b and $OTI_{SIINFEKL}$/H2-K^d tetramers conjugated to APC were prepared by the Fred Hutch Immune Monitoring Core. All cells were stained with LIVE/DEAD fixable Aqua (405nm, cat: L34966) prior to surface or intracellular staining. UltraComp eBeads (eBioscience, cat: 01–2222) were used for all compensation. For *ex vivo* experiments, cells from either untreated mice or endogenous $CD44^-$ $CD62L^+$ $CD8^+$ T cells from the spleen of treated mice were used for negative controls and gating. For *in vitro* experiments, fluorescence minus one or irrelevant engineered T cells were used for negative controls and gating.

See Supplemental Table 5 or DOI for antibody information: dx.doi.org/10.17504/protocols.io.2idgca6

Intracellular cytokine staining (ICS)

See DOI for T-cell ICS: dx.doi.org/10.17504/protocols.io.sqdeds6

Cytotoxicity assays

Tumor cells were co-cultured with transduced T cells for 18–24 hours in 24-well tissue culture plates. Target cells were then gently removed (0.05% trypsin) and transferred to FACS tubes for intracellular cleaved-caspase 3 (CC3) staining. The BD Fix/Perm kit (cat: 554714) was used for staining with anti-CC3.

See DOI for xCELLigence assay: dx.doi.org/10.17504/protocols.io.sqkeduw

Western blot

See DOI for protein extraction and western blot: dx.doi.org/10.17504/protocols.io.sqgedtw

Gene expression

RNA was extracted from fresh frozen $ID8_{VEGF}$ tumors, primary human HGSOC, metastatic HGSOC, or adjacent normal tissue from patients using the Qiagen RNeasy Plus Mini RNA isolation kit (cat: 74134). RNA samples were processed using the Clariom D Pico mouse or human Assay respectively. Arrays were analyzed using SST-RMA algorithm in the Affymetrix Transcriptome Analysis Console (TAC) Software. All samples passed the quality control criteria given by Affymetrix. Expression was then imported into R. Probes with less than two arrays above the 95^{th} percentile of the antigenomic background probes were

filtered out, leaving 18,122 and 16,806 expressed genes in human and mouse tumors, respectively.

Single-sample gene set enrichment analysis

To compare tumor types, single sample GSEA, which is an extension of GSEA that calculates separate enrichment scores for each pairing of a sample and gene set, was performed (21). Each gene set's enrichment score represents the activity level of the biological process in which the gene set's members are coordinately up- or down-regulated. The GSVA R package (V1.26.0) was used to calculate normalized enrichment scores for gene sets belonging to KEGG and REACTOME for all human and mouse tumor types. These gene sets were downloaded from MSigDB database version 6.1.

To look at differences between tumor types, we leveraged the limma R package (v3.34.9) (22). A linear model was fitted to each pathway, and empirical Bayes moderated t-statistics were used to assess differences in gene set enrichment scores. Contrasts comparing tumor types (mouse tumors, primary human tumors, and metastatic human tumors) were tested. Intra-class correlations were estimated using the duplicate Correlation function of the limma package to account for measures originating from the same donors when looking at differences between human tumor types. A false discovery rate (FDR) cutoff of 1% was used to determine differentially expressed gene sets.

Data and software availability

The microarray data have been deposited in NCBI GENE Expression Omnibus (accession numbers GSE120263 and GSE120264).

Statistics

The Student *t* test was used to compare normally distributed two-group data. A one-way Anova with post-hoc analysis pairwise for multiple comparisons was used to compare data from experiments with more than two groups. Survival curve analysis was performed using the Log-rank (Mantel-Cox) and Gehan-Breslow-Wilcoxon tests. In all box and whisker plots, the ends of the box represent the upper and lower quartiles, the median is demarcated by the center line, and the whiskers represent the highest and lowest values. All error bars represent standard deviation (SD).

RESULTS

T cells engineered to express a human MSLN-specific TCR lyse HGSOC cell lines

We previously developed HLA-A02*01 (A2)restricted TCRs that recognize either the epitope from human MSLN residues 20–28 or 530–538 (19). Primary human CD8 T cells transduced with the $MSLN_{20}$- or $MSLN_{530}$-specific TCR produced IFNγ and TNFα after stimulation with phorbol-myristate-acetate/ionomycin (PMA/I) or cognate peptide (Fig. 1A), and bound tetramers of cognate peptide:MHC (Fig. 1B). The $MSLN_{530}$ T cells exhibited lower avidity for tetramer than $MSLN_{20}$ T cells, indicating possible TCR affinity/avidity differences for peptide:MHC. The functional capacity of the $MSLN_{20}$ and $MSLN_{530}$ TCRs were tested after expression in Jurkat nur77-mCherry reporter cells, which express mCherry

proportional to TCR signal strength, and 24-hour co-culture with T2 cells pulsed with titrating peptide (Fig. 1C). Relative to $MSLN_{530}$ TCR T cells, $MSLN_{20}$ TCR T cells expressed higher levels of nur77-mCherry following stimulation, suggesting greater sensitivity to cognate Ag.

To confirm MSLN-specific T cells can recognize endogenously processed and presented antigen, $MSLN_{20}$ or $MSLN_{530}$ TCR-transduced primary human CD8 T cells were co-cultured with HLA-$A2^+$ $MSLN^+$ HGSOC cells. Many HGSOC lines are commercially available; we chose eight that best reflect the genetic profile considered typical of high grade serous disease (23). We characterized each for expression of class I MHC and MSLN (Supplementary Fig. S1A,B) and distinct HLA alleles (Table 1). MSLN expression was evaluated by intracellular staining, because adherent cells were released with trypsin, which cleaves MSLN from the cell surface (24). All eight lines were $MSLN^+$. Engineered T cells expressing either MSLN-specific TCR proliferated in response to peptide-pulsed T2 cells (Fig. 1D) or OVCAR3 HGSOC cells (Fig. 1E), and were tumoricidal, inducing expression of cleaved caspase 3 (CC3) in three $MSLN^+$ HLA-$A2^+$ HGSOC cell lines (OVCAR3, COV318, and TYKNU; Fig. 1F and Supplementary Fig. S1C). $MSLN_{20}$ and $MSLN_{530}$ TCRs are being further evaluated for clinical translation.

$ID8_{VEGF}$ tumors overexpress Msln

To assess the potential antitumor activity and possible toxicities *in vivo* of targeting MSLN, we generated immunocompetent ovarian tumor-bearing mice with advanced stage disease. $ID8_{VEGF}$ cells (17) were injected intraperitoneally (i.p.) into 7 to 8-week-old female C57BL/6J mice; ~6–8 weeks later, tumor nodules were present throughout the peritoneal cavity and detectable by high resolution ultrasound (Fig. 2A). Tumor progression produced terminal hemorrhagic ascites (Fig. 2B) detected at 10–12 weeks after tumor injection, as described (18).

Expression of MSLN, deemed a priority antigen for immunotherapy (12), was assessed by IHC or western blot in murine $ID8_{VEGF}$ tumors resected >7 weeks after tumor cell injection (Fig. 2C). Expression was higher than in healthy lung, ovary, or oviduct tissue (equivalent of human Fallopian tubes) in nontumor bearing mice (Fig. 2D).

Engineered Mouse TCR-T cells respond to TCR signals

We previously developed an affinity-enhanced murine TCR (TCR_{1045}) specific for the $Msln_{406–414}$ epitope; CD8 TCR_{1045}-T cells mediate activity against pancreatic cancer without toxicity to normal tissues (19). For the current study, we transduced naive transgenic P14 CD8 T cells, which express a TCR (TCR_{gp33}) specific for the gp33–41 epitope of lymphocytic choriomeningitis virus, with either TCR_{1045} or a tumor-irrelevant control TCR (TCR_{OTI}) specific for the ovalbumin SIINFEKL ($OVA_{257–264}$) epitope (Supplementary Fig. S2A). After TCR transduction, T cells expressed TCR_{gp33} and either TCR_{1045} or TCR_{OTI} (Supplementary Fig. S2B) and bound tetramers containing $Msln_{406–414}$ and H2-D^b or $OVA_{257–264}$ and H2-K^b, respectively (Supplementary Fig. S2C). Transduced T cells secreted IFNγ and TNFα upon encounter with their specific Ags *in vitro* (Supplementary Fig. S2D), demonstrating effector functions in response to stimulation through the engineered TCR.

Msln-specific T cells recognize and lyse ID8 ovarian cancer cells *in vitro*

To evaluate if TCR_{1045}-engineered T cells could recognize Msln naturally presented by $ID8_{VEGF}$ cells, we first confirmed $ID8_{VEGF}$ cells express H-$2D^b$ and H-$2K^b$, which can be increased by exposure to only 10ng IFNγ for 24 hours (Fig. 2E). We next evaluated activation of Msln-specific T cells after co-culture with $ID8_{VEGF}$ cells. TCR_{1045} T cells, but not TCR_{OTI} T cells, proliferated after 5 days in co-culture with tumor cells (Fig. 2F), and were cytotoxic to tumor cells, as reflected by CC3 levels in $ID8_{VEGF}$ cells after co-culture with engineered TCR_{1045} T cells compared to control TCR_{OTI} T cells (Fig. 2G). Specific lysis of $ID8_{VEGF}$ targets was proportional to the effector:target ratio (Fig. 2H); $ID8_{VEGF}$ cell death, as measured by live cell quantification, was significantly increased when tumor cells were co-cultured with TCR_{1045} versus control TCR_{OTI} T cells (Fig. 2I). All cytotoxicity experiments were also performed after pre-treatment of tumor cells with 10ng IFNγ for 24 hours to increase expression of MHC I (to determine if low MHC reduced killing); no significant increase in specific target cell cytolysis by irrelevant TCR_{OTI} cells or TCR_{1045} T cells was observed (Fig. 2I).

As immunogenicity of mouse and human cell lines can be influenced by expression of co-stimulatory and inhibitory molecules, we also evaluated expression of CD80, CD86, PD-L1, and PD-L2 on both $ID8_{VEGF}$ and OVCAR3 target cell lines. Both cell lines expressed low basal amounts of CD80, CD86, PD-L1, and PD-L2 (Supplementary Fig. S3).

$ID8_{VEGF}$ tumors recapitulate the gene expression profile of human metastatic tumors

Gene expression by $ID8_{VEGF}$ and human HGSOC tumors was compared following deep transcriptome profiling on fresh frozen patient samples (including primary tumors, metastatic omental tumors and matched adjacent normal tissue) and murine tumor masses growing in the peritoneal cavity. All human tumors were classified as HGSOC by the surgical team upon resection. We found that *Pax8* expression was not significantly different in primary and metastatic human tumor samples relative to normal fallopian tube tissue, but was elevated relative to normal ovarian tissue, suggesting the evaluated tumors may be derived from fallopian tube epithelia, considered common for HGSOC (25). As coordinately up- or down-regulated pathway-associated gene sets can influence efficacy of adoptive T-cell therapy, gene sets, defined using the Kyoto Encyclopedia of Genes and Genomes (KEGG) database (dx.doi.org/10.17504/protocols.io.2h5gb86), were evaluated using single-sample Gene Set Enrichment Analysis (ssGSEA). For consistency, all analyzed metastatic human tumors were obtained from the omentum, since tumors at different sites may acquire environmentally-induced gene expression patterns (26). Mouse genes without human orthologs (and vice versa) were excluded from the analysis. Of the 177 KEGG pathways evaluated, 138 were not significantly different between $ID8_{VEGF}$ and human tumors (Fig. 3A); 18 were significantly different in $ID8_{VEGF}$ compared to both human primary and metastatic tumors (Fig. 3B), 19 were significantly different between $ID8_{VEGF}$ and primary human tumors but not metastatic omental tumors (Fig. 3C), and 2 KEGG pathways were significantly different between $ID8_{VEGF}$ and human metastatic omental tumors but not primary human tumors (Fig. 3D). The majority of species-distinct pathways involved DNA repair or cellular metabolic processes. Although our analysis revealed several differences in gene expression between the $ID8_{VEGF}$ model and human ovarian tumors, the majority of

Ag-presentation and immunosuppressive pathways were similarly expressed in the preclinical model and patient metastatic samples. Thus, the transplantable $ID8_{VEGF}$ model could prove useful for studying human ovarian tumor-targeting immunotherapy strategies. Similar findings were obtained when ssGSEA was performed with the REACTOME database (Supplementary Fig. S4, dx.doi.org/10.17504/protocols.io.2jvgcn6).

Murine $ID8_{VEGF}$ tumors and human HGSOC share many TME inhibitory pathways

To more precisely test if immunosuppressive cells and expression of proteins that inhibit antitumor immune responses in the $ID8_{VEGF}$ TME recapitulate features of the immunosuppressive TME in human ovarian cancer, IHC was used to characterize myeloid cell (CD68), regulatory T-cell (FoxP3), and B-cell (CD20) infiltration in metastatic HGSOC tissue samples obtained from 28 patients. In patient and $ID8_{VEGF}$ tumor samples, we also measured expression of inhibitory ligands including PD-L1, CD47, galectin-9, and galectin-3. All three immunosuppressive cell types and the inhibitory ligands were present within both the mouse model and human disease (Fig. 4A), and all except $FoxP3^+$ were present in a similar proportion of mouse samples as in metastatic patient samples (Fig. 4B). As previously reported, not all patient samples exhibit accumulation of $FoxP3^+$ T cells, with $FoxP3^+$ tumor samples associated with a worse prognosis (27). However, all mouse samples reproducibly exhibited infiltration of $FoxP3^+$ T cells. Thus, the $ID8_{VEGF}$ pre-clinical model should provide opportunities to assess clinically relevant TME-targeting strategies directed at reducing the activity of the major immune suppressive cell types and enhancing the efficacy of T cell-based therapies.

Tumor-specific engineered T cells are enriched in $ID8_{VEGF}$ tumors

To further evaluate Msln-targeting T cell therapy of late-stage disease, we transferred transduced TCR_{1045} or TCR_{OTI} T cells (1×10^7) intravenously (i.v.) into $ID8_{VEGF}$ ovarian tumor-bearing mice, after metastatic peritoneal tumors were detectable by ultrasound (at ≥ 6 weeks after tumor cell injection). Tumor-specific TCR_{1045} T cells showed preferential accumulation in $ID8_{VEGF}$ tumors at day 7 compared to spleen or blood (Fig. 5A). In contrast, TCR_{OTI} T cells showed greater than four-fold reduced accumulation in the tumor (3.23 vs. 14.31, with total T cells in the tumor ten-fold lower, p=0.0042). The limited tumor infiltration in TCR_{OT} T cell treated mice potentially reflects non-specific attraction to an inflammatory site (Fig. 5B). The transferred TCR_{1045} population was detectable within tumors 7 days after injection (Supplementary Fig. S5A), but thereafter underwent contraction, becoming undetectable after 28 days (Supplementary Fig. S5B). To evaluate engineered T cell proliferation within the tumor, cells were Ki67 stained prior to transfer or following isolation from tumors eight days after transfer. Engineered T cells were $Ki67^+$ prior to cell transfer, but $Ki67^-$ after eight days (Supplementary Fig. S5C), suggesting limited CD8 T-cell proliferation within $ID8_{VEGF}$ tumors. A single dose of TCR_{1045} T cells did not significantly increase survival in tumor-bearing mice.

To enhance tumor-specific donor T-cell enrichment within tumors, we immunogenically stimulated the transferred T cells with peptide-pulsed, irradiated splenocytes as a “vaccine” post-transfer (Fig. 5C). However, *in vivo* persistence of transferred T cells remained poor; as early as three weeks after transfer, donor cells were difficult to detect in peripheral blood,

spleen and tumors (Fig. 5D). Transient depletion of the host T-cell compartment with chemotherapeutic regimens prior to T-cell transfer can promote homeostatic proliferation and improve donor T-cell persistence (28) and efficacy (29). Therefore, we lymphodepleted recipient mice with cyclophosphamide (180 mg/kg) >6 hours prior to the initial T-cell injection and vaccination, to allow for clearance of the drug, which increased both the intratumoral proportion of donor T cells (Fig. 5E) and persistence of intratumoral transferred T-cells at 21 days post-transfer (Fig. 5D). The chemotherapy had only a transient effect on other infiltrating immune cells; the number of myeloid-derived cells isolated from $ID8_{VEGF}$ tumors was significantly reduced 12 hours after cyclophosphamide-induced lymphodepletion, including total $CD11b^+$ cells, $CD11b^+Ly6G^+Ly6C^{low}$ granulocytic-myeloid derived suppressor cells (Gr-MDSC), and $CD11b^+Ly6C^+Ly6G^-$ monocytic-MDSC (Mo-MSDC) (Supplementary Fig. S6A), but this number rebounded within 7 days and was then either slightly (total $CD11b^+$ cells, Gr-MDSC) or significantly (Mo-MDSC) increased relative to untreated tumors (Supplementary Fig. S6B), consistent with previous reports (30). The number of regulatory T cells (Tregs) isolated from tumors was also significantly reduced 12 hours post-lymphodepletion (Supplementary Fig. S6C), but did not differ between treated and untreated mice at 7 days post-lymphodepletion (Supplementary Fig. S6D), suggesting lymphodepletion had at most only a transient effect on immunosuppressive populations.

Msln-specific T cells upregulate expression of exhaustion markers over time

To evaluate if tumor-infiltrating T cells recognize and respond to $ID8_{VEGF}$ tumor cells *in vivo*, we examined expression of classic activation markers on TCR_{1045} T cells isolated from spleen or tumor seven days after T-cell transfer. Proteins associated with recent and sustained T-cell activation (CD69, CD137/4–1BB, PD-1, Lag-3, Tim-3, TIGIT) were significantly elevated on transferred TCR_{1045} T cells isolated from tumors compared to cells from spleen (Fig. 5F). These activation/exhaustion molecules remained elevated on TCR_{1045} T cells isolated from tumors 21 days post-transfer (Fig. 5G), suggesting intra-tumoral TCR_{1045} T cells were experiencing chronic antigen stimulation and exhaustion, consistent with reports of T-cell dysfunction in other solid tumor models (19,31,32).

Tumor-infiltrating T cells isolated from treated mice at seven days post-transfer still produced antitumor cytokines when exposed to cognate peptide *ex vivo*, although this was trending lower than in donor T cells isolated from spleen (Fig. 5H). However, at 21 days post-transfer, fewer engineered T cells retained the ability to produce cytokine in response to antigen, and only at lower levels (Fig. 5H,I), suggesting that T cells became dysfunctional in the $ID8_{VEGF}$ TME, consistent with the exhaustion marker expression.

A combinatorial therapeutic regimen delays tumor growth and promotes survival

Because the transferred T cells exhibited numerical decline and loss of function within 21 days of transfer, we examined if repeated doses of functional T cells could enhance therapeutic efficacy. To evaluate tumor control and overall survival, we lymphodepleted tumor-bearing mice once and then transferred engineered T cells along with an irradiated peptide-pulsed splenocyte vaccine every 14 days, as we described previously for treating pancreatic cancer (19). A second dose of TCR_{1045} T cells also infiltrated $ID8_{VEGF}$ tumors

when infused with vaccine 14 days after the initial T-cell transfer (Supplementary Fig. S7A). Moreover, the vaccine may have increased the number of intratumoral T cells derived from the initial T-cell transfer, presumably by boosting functional T cells in secondary lymphoid organs (Supplementary Fig. S7B). Mice treated with TCR_{1045} T cells had a significant survival advantage (defined as time to progression with terminal hemorrhagic ascites, our defined euthanasia criteria) compared to untreated mice (Fig. 6A; untreated/treated median survival = 77/112 days). Mice treated with serial infusions (but with no lymphodepletion or *in vivo* vaccine) also showed significantly prolonged survival (Fig. 6B, untreated/treated median survival = 77/91 days), but this improvement was more modest than with the vaccine-inclusive treatment regimen. TCR_{OTI} T cells plus Msln vaccine did not significantly prolong survival (Supplementary Fig. S7C). At necropsy, we saw no evidence of T-cell accumulation or injury at Msln-expressing mesothelial surfaces (Supplementary Fig. S7D,E), as we previously reported (19).

One week after the third T-cell administration, cohorts of mice were euthanized to examine tumor cell killing with CC3 staining. Significantly increased CC3 staining (Fig. 6C,D) was observed in tumors from mice treated with TCR_{1045} T cells ($p = 0.038$) compared to untreated controls, whereas tumors from untreated mice and mice treated with TCR_{OTI} T cells were not different, affirming that prolonged survival after T-cell therapy reflected antigen-specific antitumor activity. As all mice ultimately succumbed to progressive disease with this treatment regimen, we evaluated if this reflected limitations of the regimen in advanced disease or was due to loss of antigen expression in the tumor. Tumors were analyzed from mice euthanized after three T-cell administrations, the latest time point at which mice treated with control T cells were predictably alive; no significant difference in Msln expression was observed in TCR_{1045}–treated tumors relative to untreated or TCR_{OTI}–treated tumors (Fig. 6E,F).

DISCUSSION

Despite abundant evidence that ovarian cancer can be immunogenic, efforts to harness endogenous immune responses have been largely ineffective (33). Here we demonstrate that adoptive therapy with T cells engineered with a high-affinity Msln-targeting TCR prolong survival of mice harboring late-stage metastatic disease, a setting resembling tumors in advanced-stage HGSOC patients (33). Treatment spared the normal tissues in which Msln is also expressed (13), as was seen in Msln-specific TCR-treated pancreatic cancer (19). We found that the $ID8_{VEGF}$ transplantable tumor model recapitulates many molecular characteristics of the human disease, as well as hallmarks of advanced stage ovarian cancer, including aggressive growth, peritoneal dissemination and terminal hemorrhagic ascites. $ID8_{VEGF}$ tumors, similar to human tumors, also overexpress Msln. Similar to human ovarian cancer cell lines, $ID8_{VEGF}$ expresses low basal MHC class I, which increased upon exposure to IFNγ, which is produced by infiltrating T cells, suggesting initially low class I expression is not an insurmountable obstacle for TCR-based targeting.

Although findings in preclinical models that recapitulate TME features of human tumors should have improved potential for direct translation to the clinic, this is not always the case, perhaps due to differing murine and human evolutionary genetics (34), pathogen exposure

(35), microbiome composition (36), and immune system development (37). Thus, understanding a model system's limitations is critical for rational data interpretation and translation. Our comparison of deep transcriptome profiles revealed similar expression of most pathways that impact efficacy of T cell-based immunotherapies, including antigen processing and presentation, and VEGF, TGF-β, WNT, cytokine, and chemokine signaling pathways. Metabolic and xenobiotic studies in the $ID8_{VEGF}$ model may be less broadly predictive for human high grade serous ovarian cancer, due to significantly higher expression of the cytochrome P450 family and numerous metabolic pathways in $ID8_{VEGF}$ tumors versus human HGSOC. For example, IDO inhibitor studies in the $ID8_{VEGF}$ model may be applicable only to the subset of ovarian cancers that also have high IDO expression (38).

Genetic mutations that disrupt DNA repair pathways are detected in a subset of ovarian cancer patients, and are a major target of emerging chemotherapies (39), but are not present in the $ID8_{VEGF}$ model. Studies combining immunotherapy with DNA repair pathway targeting, such as with poly(ADP-ribose) polymerase inhibitors, may be more informative in recent ID8 models genetically engineered to disrupt DNA repair mechanisms, such as the CRISPR/Cas9-modifed ID8 line containing *Trp53* and *Brca1* or *Trp53* and *Brca2* mutations (40).

Despite these limitations, many immunosuppressive mechanisms described for human ovarian cancer are present in $ID8_{VEGF}$ tumors. In our studies, high expression of CD69, CD137, PD-1, Lag-3, Tim-3, and TIGIT was detected on engineered tumor-infiltrating T cells three weeks after T-cell administration, consistent with the T cells experiencing chronic TCR signaling. These T cells also exhibited diminished function, as predicted by this exhaustion-associated phenotypic signature (41,42). Thus, the $ID8_{VEGF}$ model may be suitable for assessing if adding checkpoint blockade would be a useful strategy to build on our initial results with T-cell therapy, but more than one checkpoint inhibitor may be required to achieve efficacy in advanced stage disease. Further, expression of Fas Ligand in the vasculature of human and murine $ID8_{VEGF}$ ovarian tumors correlates with reduced CD8 T-cell infiltration/survival (43), which may also diminish efficacy of engineered adoptive T-cell therapy. Thus, strategies for overcoming this immune-evasion mechanism may also be evaluated using the $ID8_{VEGF}$ model. Overexpression of metabolic pathways in $ID8_{VEGF}$ tumors suggests that a nutrient-depleted, metabolically active TME may also contribute to intra-tumoral T-cell dysfunction, which could be experimentally explored.

Suppressive intratumoral leukocytes can also inhibit CD8 T-cell function. Tregs, MDSC, and tumor-associated macrophages (TAM) accumulate in the ovarian cancer TME and can dampen antitumor responses (33,44). The presence of these suppressive immune cells in the $ID8_{VEGF}$ TME further suggests this model may be informative for studies involving depletion or modulation of suppressive cells or further engineering T cells to be resistant to suppressive factors produced by these cells.

We also found that human T cells engineered to express a high-affinity tumor-specific TCR specifically induce apoptosis of three different HLA-A02*01^{+} MSLN-expressing ovarian cancer cell lines that molecularly resemble HGSOC (23), with some differences in susceptibility. Strategies that enhance antigen processing and presentation, such as

administration of interferons or TLR or STING agonists, may further improve susceptibility of patient tumor cells to TCR-transduced T cells.

No off-tumor on-target toxicities were observed in our preclinical studies, consistent with the acceptable Phase I and II safety profiles reported for targeting MSLN with either a monoclonal MSLN-specific monoclonal antibody (13) or heterologous prime-boost vaccinations to MSLN (45). However, as single modality treatments, these approaches have had only modest benefits. Phase I studies with MSLN-targeting CAR T cells have also shown some evidence of antitumor responses (46), but had immunogenicity issues and unclear risks of toxicity to normal tissues (47). Overall, current clinical and preclinical data suggest MSLN may be safely targeted with TCR-engineered T cells, and that use of fully human TCRs has the potential to establish detectable, persistent and functional antitumor responses.

Immunocompetent preclinical models provide an opportunity to evaluate the efficacy and safety of adoptive T-cell therapy *in vivo*, and to elucidate and address obstacles to efficacy. Our results represent a proof-of-concept that ovarian cancer can be targeted with TCR-engineered CD8 T cells to achieve clinical benefit, but also suggest therapy with adoptive transfer of high-affinity T cells alone may be insufficient to eradicate advanced disease. For example, the data from our repeated infusion studies suggests subsequent T-cell injections may have reduced tumor infiltration or accumulation compared to the initial injection. The mechanism(s) underlying this observation requires further investigation. The $ID8_{VEGF}$ model also provides an opportunity for evaluating additional engineering approaches for overcoming TME obstacles to antitumor T-cell function. For example, as TCR_{1045} can recognize peptide:MHC I in the absence of CD8 (19), engineering CD4 T cells to include expression of this TCR and co-transferring such engineered CD4 and CD8 T cells may improve antitumor efficacy, as seen with CD4 and CD8 CAR-T cells targeting leukemia (48). Alternatively, T cells engineered to express a high-affinity TCR may be further engineered to express synthetic immunomodulatory fusion proteins (IFP) that replace an inhibitory receptor with a fusion protein that retains the receptor ectodomain but has a substitute cytoplasmic tail that provides an activation or survival signal (8). Such IFPs may simultaneously enhance co-stimulatory signaling and act as a dominant negative signal (reducing the endogenous negative stimuli received by the T cell). Thus, development of an optimally effective T cell-based therapy for ovarian cancer will likely require iterative studies in patients and informative mouse models, such as the $ID8_{VEGF}$ model.

Supplementary Material

Refer to Web version on PubMed Central for supplementary material.

ACKNOWLEDGEMENTS

This work was supported by the Chromosome Metabolism and Cancer Training Grant Program (T32 2T32CA009657-26A1 to K.G.A), the Ovarian Cancer Research Alliance (K.G.A.), a Solid Tumor Translational Research Award (to K.G.A. and P.D.G.), the NIH National Cancer Institute (CA018029 and CA033084 to P.D.G), the Leukemia & Lymphoma Society (S.K.O.), and a research agreement with Juno Therapeutics and the Parker Institute for Cancer Immunotherapy (to P.D.G.). The content is solely the responsibility of the authors and does not necessarily represent the official views of the NIH.

The authors thank Matthias Stephan for the ID8$_{VEGF}$ cell line; Sunni Farley, Robert Pierce, Savanh Chanthaphavong, Brian Johnson and Megan Larmore for histopathology assistance; Frank Carbone for TCR$_{OTI}$ construct development; Thomas Schmitt for MSLN-specific TCR development; Magdalia Suarez, Andrew Daman, Lara Kropp and Rachel Perret for assistance with experiments; the Fred Hutchinson Cancer Research Center Flow Cytometry Core for technical support; Deborah Banker for critical review of the manuscript; and all members of the Greenberg lab for thoughtful and critical discussion.

Financial support: This work was supported by the Chromosome Metabolism and Cancer Training Grant Program (T32 2T32CA009657-26A1 to K.G.A), a Solid Tumor Translational Research Award (to K.G.A. and P.D.G.), the NIH National Cancer Institute (CA018029 and CA033084 to P.D.G), the Leukemia & Lymphoma Society (S.K.O.), and a research agreement with Juno Therapeutics (to P.D.G.). The content is solely the responsibility of the authors and does not necessarily represent the official views of the NIH.

REFERENCES

1. Lheureux S, Karakasis K, Kohn EC, Oza AM. Ovarian cancer treatment: The end of empiricism? Cancer. 2015;121:3203–11. [PubMed: 26096019]
2. Vaughan S, Coward JI, Bast RC, Berchuck A, Berek JS, Brenton JD, et al. Rethinking ovarian cancer: recommendations for improving outcomes. Nat Rev Cancer. Nature Publishing Group; 2011 pages 719–25. [PubMed: 21941283]
3. Zsiros E, Tanyi J, Balint K, Kandalaft LE. Immunotherapy for ovarian cancer: recent advances and perspectives. Curr Opin Oncol. 2014;26:492–500. [PubMed: 25036883]
4. Santoiemma PP, Powell DJ. Tumor infiltrating lymphocytes in ovarian cancer. Cancer Biol Ther. 2015;16:807–20. [PubMed: 25894333]
5. Dembić Z, Haas W, Weiss S, McCubrey J, Kiefer H, Boehmer von H, et al. Transfer of specificity by murine alpha and beta T-cell receptor genes. Nature. 1986;320:232–8. [PubMed: 2421164]
6. Prosser ME, Brown CE, Shami AF, Forman SJ, Jensen MC. Tumor PD-L1 co-stimulates primary human CD8+ cytotoxic T cells modified to express a PD1:CD28 chimeric receptor. Molecular Immunology. Elsevier Ltd; 2012;51:263–72. [PubMed: 22503210]
7. Su S, Hu B, Shao J, Shen Bin, Du J, Du Y, et al. CRISPR-Cas9 mediated efficient PD-1 disruption on human primary T cells from cancer patients. Sci Rep. Nature Publishing Group; 2016;:1–14. [PubMed: 28442746]
8. Oda SK, Daman AW, Garcia NM, Wagener F, Schmitt TM, Tan X, et al. A CD200R-CD28 fusion protein appropriates an inhibitory signal to enhance T-cell function and therapy of murine leukemia. Blood. American Society of Hematology; 2017;130:2410–9. [PubMed: 29042364]
9. Morello A, Sadelain M, Adusumilli PS. Mesothelin-Targeted CARs: Driving T Cells to Solid Tumors. Cancer Discov. 2016;6:133–46. [PubMed: 26503962]
10. Chodon T, Comin-Anduix B, Chmielowski B, Koya RC, Wu Z, Auerbach M, et al. Adoptive transfer of MART-1 T-cell receptor transgenic lymphocytes and dendritic cell vaccination in patients with metastatic melanoma. Clin Cancer Res. 2014;20:2457–65. [PubMed: 24634374]
11. Robbins PF, Morgan RA, Feldman SA, Yang JC, Sherry RM, Dudley ME, et al. Tumor regression in patients with metastatic synovial cell sarcoma and melanoma using genetically engineered lymphocytes reactive with NY-ESO-1. J Clin Oncol. 2011;29:917–24. [PubMed: 21282551]
12. Cheever MA, Allison JP, Ferris AS, Finn OJ, Hastings BM, Hecht TT, et al. The Prioritization of Cancer Antigens: A National Cancer Institute Pilot Project for the Acceleration of Translational Research. Clin Cancer Res. 2009;15:5323–37. [PubMed: 19723653]
13. Hassan R, Thomas A, Alewine C, Le DT, Jaffee EM, Pastan I. Mesothelin Immunotherapy for Cancer: Ready for Prime Time? J Clin Oncol. 2016;34:4171–9. [PubMed: 27863199]
14. Boegel S, Löwer M, Bukur T, Sorn P, Castle JC, Sahin U. HLA and proteasome expression body map. BMC Med Genomics. BioMed Central; 2018;11:36. [PubMed: 29587858]
15. Pastan I, Zhang Y. Modulating mesothelin shedding to improve therapy. Oncotarget. Impact Journals; 2012;3:114–5. [PubMed: 22337812]
16. Roby KF, Taylor CC, Sweetwood JP, Cheng Y, Pace JL, Tawfik O, et al. Development of a syngeneic mouse model for events related to ovarian cancer. Carcinogenesis. 2000;21:585–91. [PubMed: 10753190]

17. Zhang L, Yang N, Garcia J-RC, Mohamed A, Benencia F, Rubin SC, et al. Generation of a syngeneic mouse model to study the effects of vascular endothelial growth factor in ovarian carcinoma. Am J Pathol. 2002;161:2295–309. [PubMed: 12466143]
18. Janát-Amsbury MM, Yockman JW, Anderson ML, Kieback DG, Kim SW. Comparison of ID8 MOSE and VEGF-modified ID8 cell lines in an immunocompetent animal model for human ovarian cancer. Anticancer Res. 2006;26:2785–9. [PubMed: 16886597]
19. Stromnes IM, Schmitt TM, Hulbert A, Brockenbrough JS, Nguyen HN, Cuevas C, et al. T Cells Engineered against a Native Antigen Can Surmount Immunologic and Physical Barriers to Treat Pancreatic Ductal Adenocarcinoma. Cancer Cell. Elsevier Inc; 2015;28:638–52. [PubMed: 26525103]
20. Pircher H, Michalopoulos EE, Iwamoto A, Ohashi PS, Baenziger J, Hengartner H, et al. Molecular analysis of the antigen receptor of virus-specific cytotoxic T cells and identification of a new V alpha family. Eur J Immunol. 1987;17:1843–6. [PubMed: 2961577]
21. Rahmatallah Y, Emmert-Streib F, Glazko G. Gene set analysis approaches for RNA-seq data: performance evaluation and application guideline. Brief Bioinformatics. 2016;17:393–407. [PubMed: 26342128]
22. Ritchie ME, Phipson B, Wu D, Hu Y, Law CW, Shi W, et al. limma powers differential expression analyses for RNA-sequencing and microarray studies. Nucleic Acids Res. 2015;43:e47–7. [PubMed: 25605792]
23. Domcke S, Sinha R, Levine DA, Sander C, Schultz N. Evaluating cell lines as tumour models by comparison of genomic profiles. Nature Communications. Nature Publishing Group; 2013;4:2126.
24. Zervos E, Agle S, Freistaedter AG, Jones GJB, Roper RL. Murine mesothelin: characterization, expression, and inhibition of tumor growth in a murine model of pancreatic cancer. Journal of Experimental & Clinical Cancer Research. Journal of Experimental & Clinical Cancer Research; 2016;:1–13. [PubMed: 26728266]
25. Labidi-Galy SI, Papp E, Hallberg D, Niknafs N, Adleff V, Noe M, et al. High grade serous ovarian carcinomas originate in the fallopian tube. Nature Communications. Springer US; 2017;:1–10.
26. Jiménez-Sánchez A, Memon D, Pourpe S, Veeraraghavan H, Li Y, Vargas HA, et al. Heterogeneous Tumor-Immune Microenvironments among Differentially Growing Metastases in an Ovarian Cancer Patient. Cell. 2017;170:927–938.e20. [PubMed: 28841418]
27. Curiel TJ, Coukos G, Zou L, Alvarez X, Cheng P, Mottram P, et al. Specific recruitment of regulatory T cells in ovarian carcinoma fosters immune privilege and predicts reduced survival. Nat Med. 2004;10:942–9. [PubMed: 15322536]
28. Rosenberg SA, Restifo NP, Yang JC, Morgan RA, Dudley ME. Adoptive cell transfer: a clinical path to effective cancer immunotherapy. Nat Rev Cancer. Nature Publishing Group; 2008;8:299–308. [PubMed: 18354418]
29. Wrzesinski C, Paulos CM, Kaiser A, Muranski P, Palmer DC, Gattinoni L, et al. Increased intensity lymphodepletion enhances tumor treatment efficacy of adoptively transferred tumor-specific T cells. J Immunother. Journal of Immunotherapy; 2010;33:1–7. [PubMed: 19952961]
30. Ding Z-C, Munn DH, Zhou G. Chemotherapy-induced myeloid suppressor cells and antitumor immunity: The Janus face of chemotherapy in immunomodulation. Oncoimmunology. 2014;3:e954471. [PubMed: 25610747]
31. Schietinger A, Philip M, Krisnawan VE, Chiu EY, Delrow JJ, Basom RS, et al. Tumor-Specific T Cell Dysfunction Is a Dynamic Antigen-Driven Differentiation Program Initiated Early during Tumorigenesis. Immunity. Elsevier Inc; 2016;45:389–401. [PubMed: 27521269]
32. Chen L, Flies DB. Molecular mechanisms of T cell co-stimulation and co-inhibition. Nat Rev Immunol. 2013;13:227–42. [PubMed: 23470321]
33. Motz GT, Coukos G. Deciphering and reversing tumor immune suppression. Immunity. 2013;39:61–73. [PubMed: 23890064]
34. Uhl EW, Warner NJ. Mouse Models as Predictors of Human Responses: Evolutionary Medicine. Current Pathobiology Reports. Springer US; 2015;3:219–23. [PubMed: 26246962]
35. Beura LK, Hamilton SE, Bi K, Schenkel JM, Odumade OA, Casey KA, et al. Normalizing the environment recapitulates adult human immune traits in laboratory mice. Nature. Nature Publishing Group; 2016;532:512–6. [PubMed: 27096360]

36. Nguyen TLA, Vieira-Silva S, Liston A, Raes J. How informative is the mouse for human gut microbiota research? Disease Models & Mechanisms. 2015;8:1–16. [PubMed: 25561744]
37. Bailey M, Christoforidou Z, Lewis MC. The evolutionary basis for differences between the immune systems of man, mouse, pig and ruminants. Veterinary Immunology and Immunopathology. Elsevier B.V; 2013;152:13–9. [PubMed: 23078904]
38. Inaba T, Ino K, Kajiyama H, Yamamoto E, Shibata K, Nawa A, et al. Role of the immunosuppressive enzyme indoleamine 2,3-dioxygenase in the progression of ovarian carcinoma. Gynecologic Oncology. Elsevier Inc; 2009;115:185–92. [PubMed: 19665763]
39. Mariappan L, Jiang XY, Jackson J, Drew Y. Emerging treatment options for ovarian cancer: focus on rucaparib. Int J Womens Health. Dove Press; 2017;9:913–24. [PubMed: 29290694]
40. Walton J, Blagih J, Ennis D, Leung E, Dowson S, Farquharson M, et al. CRISPR/Cas9-Mediated Trp53 and Brca2 Knockout to Generate Improved Murine Models of Ovarian High-Grade Serous Carcinoma. Cancer Res. 2016;76:6118–29. [PubMed: 27530326]
41. Ahmadzadeh M, Johnson LA, Heemskerk B, Wunderlich JR, Dudley ME, White DE, et al. Tumor antigen-specific CD8 T cells infiltrating the tumor express high levels of PD-1 and are functionally impaired. Blood. 2009;114:1537–44. [PubMed: 19423728]
42. Matsuzaki J, Gnjatic S, Mhawech-Fauceglia P, Beck A, Miller A, Tsuji T, et al. Tumor-infiltrating NY-ESO-1–specific CD8 +T cells are negatively regulated by LAG-3 and PD-1 in human ovarian cancer. Proc Natl Acad Sci USA. 2010;107:7875–80. [PubMed: 20385810]
43. Motz GT, Santoro SP, Wang L-P, Garrabrant T, Lastra RR, Hagemann IS, et al. Tumor endothelium FasL establishes a selective immune barrier promoting tolerance in tumors. Nat Med. Nature Publishing Group; 2014;20:607–15. [PubMed: 24793239]
44. Biswas SK, Mantovani A. Macrophage plasticity and interaction with lymphocyte subsets: cancer as a paradigm. Nature Immunology. Nature Publishing Group; 2010;11:889–96. [PubMed: 20856220]
45. Le DT, Wang-Gillam A, Picozzi V, Greten TF, Crocenzi T, Springett G, et al. Safety and survival with GVAX pancreas prime and Listeria Monocytogenes-expressing mesothelin (CRS-207) boost vaccines for metastatic pancreatic cancer. J Clin Oncol. 2015;33:1325–33. [PubMed: 25584002]
46. Beatty GL, Haas AR, Maus MV, Torigian DA, Soulen MC, Plesa G, et al. Mesothelin-specific chimeric antigen receptor mRNA-engineered T cells induce anti-tumor activity in solid malignancies. Cancer Immunol Res. American Association for Cancer Research; 2014;2:112–20. [PubMed: 24579088]
47. Maus MV, Haas AR, Beatty GL, Albelda SM, Levine BL, Liu X, et al. T cells expressing chimeric antigen receptors can cause anaphylaxis in humans. Cancer Immunol Res. American Association for Cancer Research; 2013;1:26–31.
48. Sommermeyer D, Hudecek M, Kosasih PL, Gogishvili T, Maloney DG, Turtle CJ, et al. Chimeric antigen receptor-modified T cells derived from defined CD8+ and CD4+ subsets confer superior antitumor reactivity in vivo. Leukemia. 2016;30:492–500. [PubMed: 26369987]

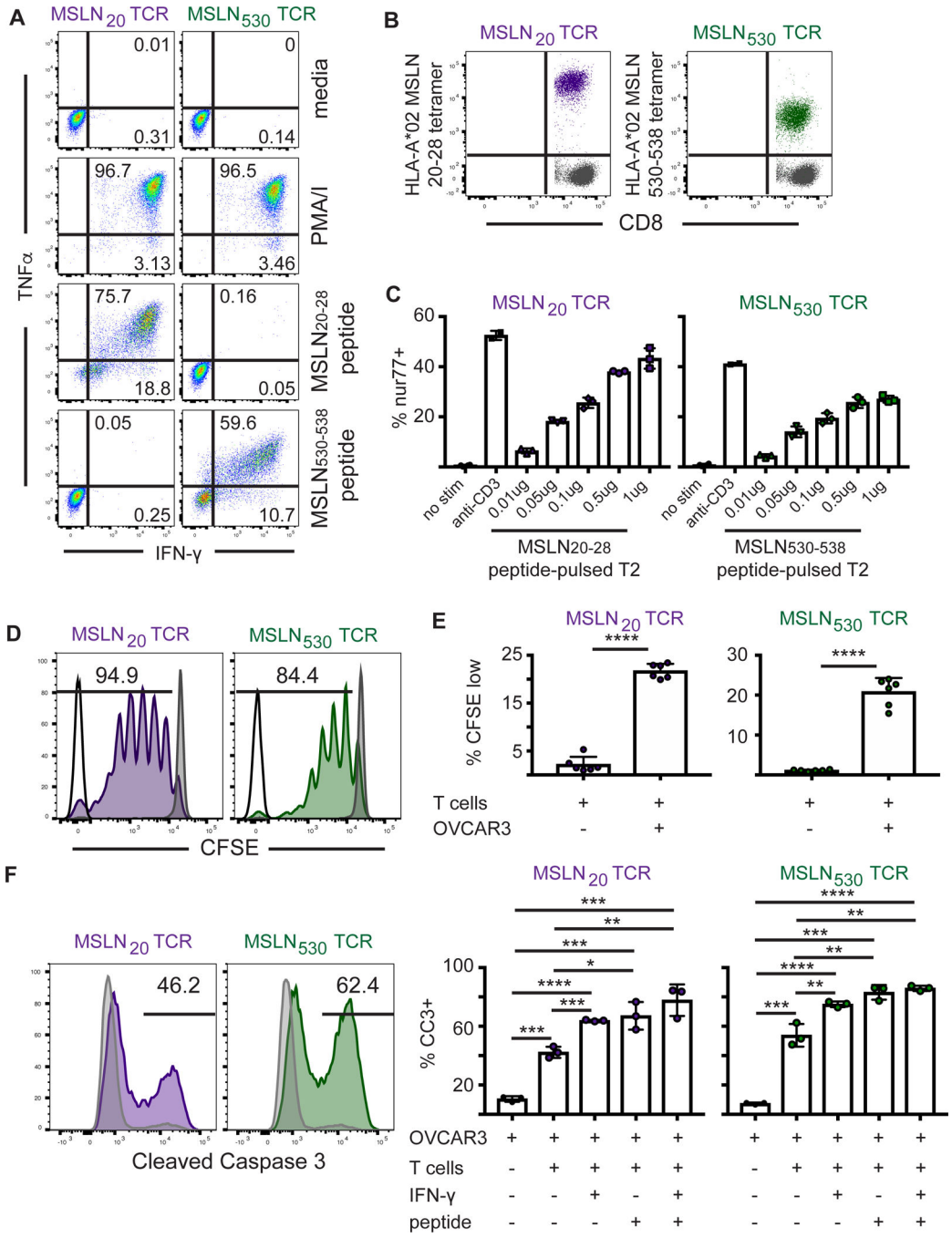

Figure 1. Engineered human MSLN-specific T cells recognize and lyse human ovarian cancer cells.

A). Intracellular cytokine staining of primary T cells engineered to express $MSLN_{20}$ or $MSLN_{530}$ TCRs. Engineered T cells were stimulated for 5 hours with PMA/I or cognate peptide and cytokine production was measured.

B) HLA-A2 tetramer staining of $MSLN_{20}$ or $MSLN_{530}$ TCR-expressing primary T cells. The gray population represents untransduced control CD8 T cells from PBMC.

C) Jurkat reporter T cells expressing $MSLN_{20}$- or $MSLN_{530}$-specific TCRs were co-cultured with peptide-pulsed HLA-$A2^+$ T2 cells for 24 hours and evaluated for induction of nur77-$mCherry^+$ expression.

D) Representative plot of CFSE dilution of $MSLN_{20}$- or $MSLN_{530}$ TCR-expressing primary T cells after co-culture with peptide-pulsed HLA-$A2^+$ T2 cells for 7 days. $MSLN_{20–28}$-specific T cells in purple. $MSLN_{530–538}$-specific T cells in green.

E) Quantitation of CFSE dilution of $MSLN_{20}$ or $MSLN_{530}$-specific TCR-expressing primary T cells after co-culture with OVCAR3 tumor cells for 7 days.

F) OVCAR3 tumor cells (with or without exposure to IFNγ at 10ng/ml for 24 hours) were pulsed with media or 1μg peptide for 90 minutes and co-cultured at a 5:1 E:T ratio with $MSLN_{20–28}$- or $MSLN_{530–538}$-specific T cells for 24 hours. Following co-culture, OVCAR3 cells were stained for Cleaved Caspase 3. Killing by $MSLN_{20–28}$-specific T cells in purple. Killing by $MSLN_{530–538}$-specific T cells in green. Gray histograms represent CC3 staining in control tumor cells. Data are shown +/− SD. All data are representative of 2–3 independent experiments.

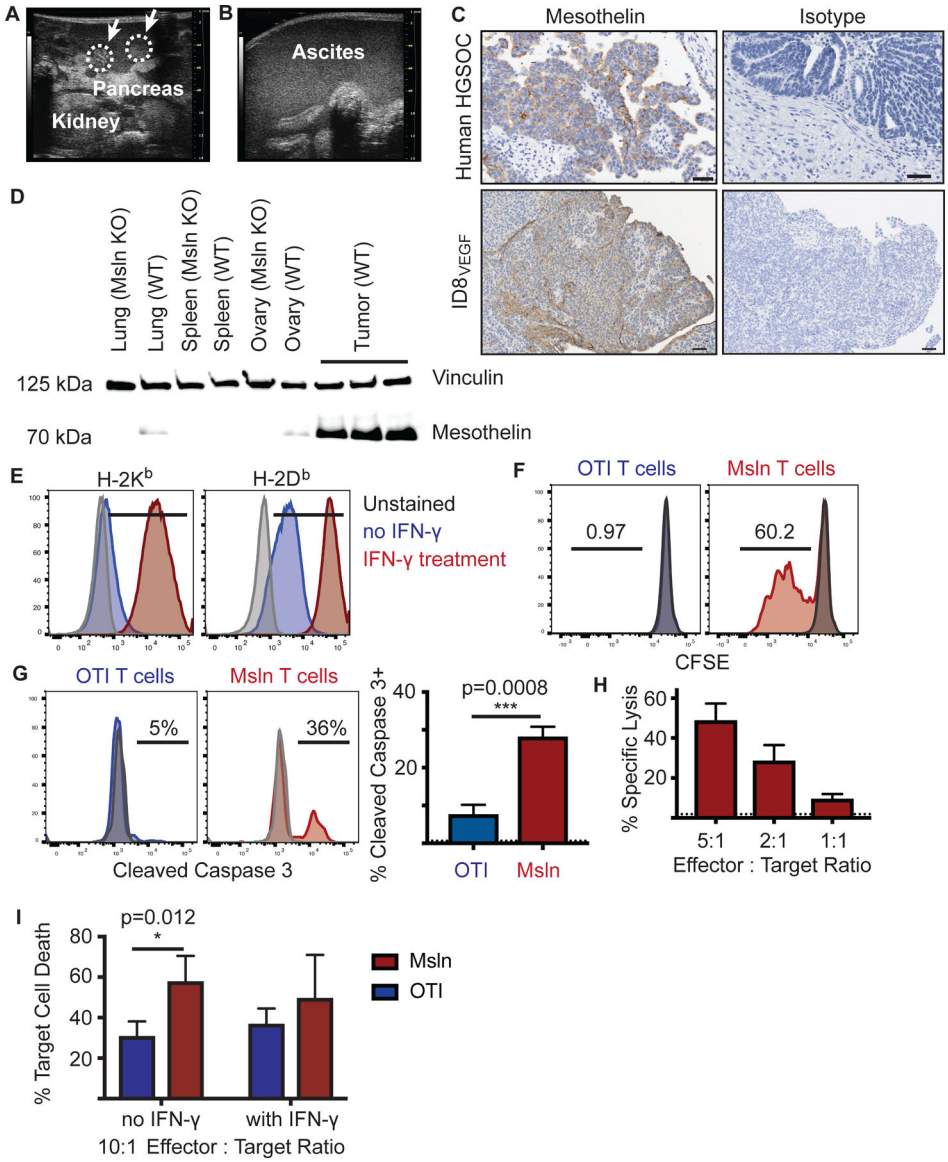

Figure 2. Engineered murine TCR_{1045} T cells lyse murine ovarian cancer cells.

A) High-resolution ultrasound of $ID8_{VEGF}$ tumor development in the peritoneal cavity (8 weeks after injection). White arrows with circles demarcate tumor nodules in the pancreas.

B) High resolution ultrasound of advanced disease. Anechoic ultrasound pattern indicates ascites development in the peritoneal cavity and obscures tissue landmarks.

C) Immunohistochemistry for MSLN/Msln in human high-grade serous ovarian cancer or $ID8_{VEGF}$ tumors. Images are representative of 15 $ID8_{VEGF}$ tumors and 31 HGSOC samples.

D) Immunoblot analyses of wild type or Msln knockout mouse tissues and $ID8_{VEGF}$ tumors for Msln protein expression. Vinculin was used as the loading control. Representative of 2 independent experiments.

E) MHC I expression on $ID8_{VEGF}$ tumor cells with or without IFNγ exposure (10ng/ml for 24 hours).

F) CFSE dilution of TCR_{1045} or control TCR_{OTI} T cells after co-culture with $ID8_{VEGF}$ tumor cells for 5 days.
G) Cleaved Caspase 3 expression in $ID8_{VEGF}$ tumor cells after co-culture with TCR_{1045} or control TCR_{OTI} T cells for 16 hours. Dotted line at 0.64% represents average frequency of $CC3^{+}$ staining in $ID8_{VEGF}$ tumor cells at the equivalent time after plating without co-culture.
H) Cytolysis of $ID8_{VEGF}$ tumor cells after co-culture with TCR_{1045} or irrelevant TCR_{OTI} T cells for 16 hours, measured by impedance of an electrical signal by target cells (xCELLigence platform). Dotted line at 1.89% represents the average background lysis by TCR_{OTI} T cells.
I) Percent of $ID8_{VEGF}$ target cell death by live cell quantification after co-culture with TCR_{1045} or control TCR_{OTI} T cells for 16 hours. All data are representative of 2–3 independent experiments. White arrows indicate tumor nodules. Scale bar = 50 microns. Data are shown +/− SD.

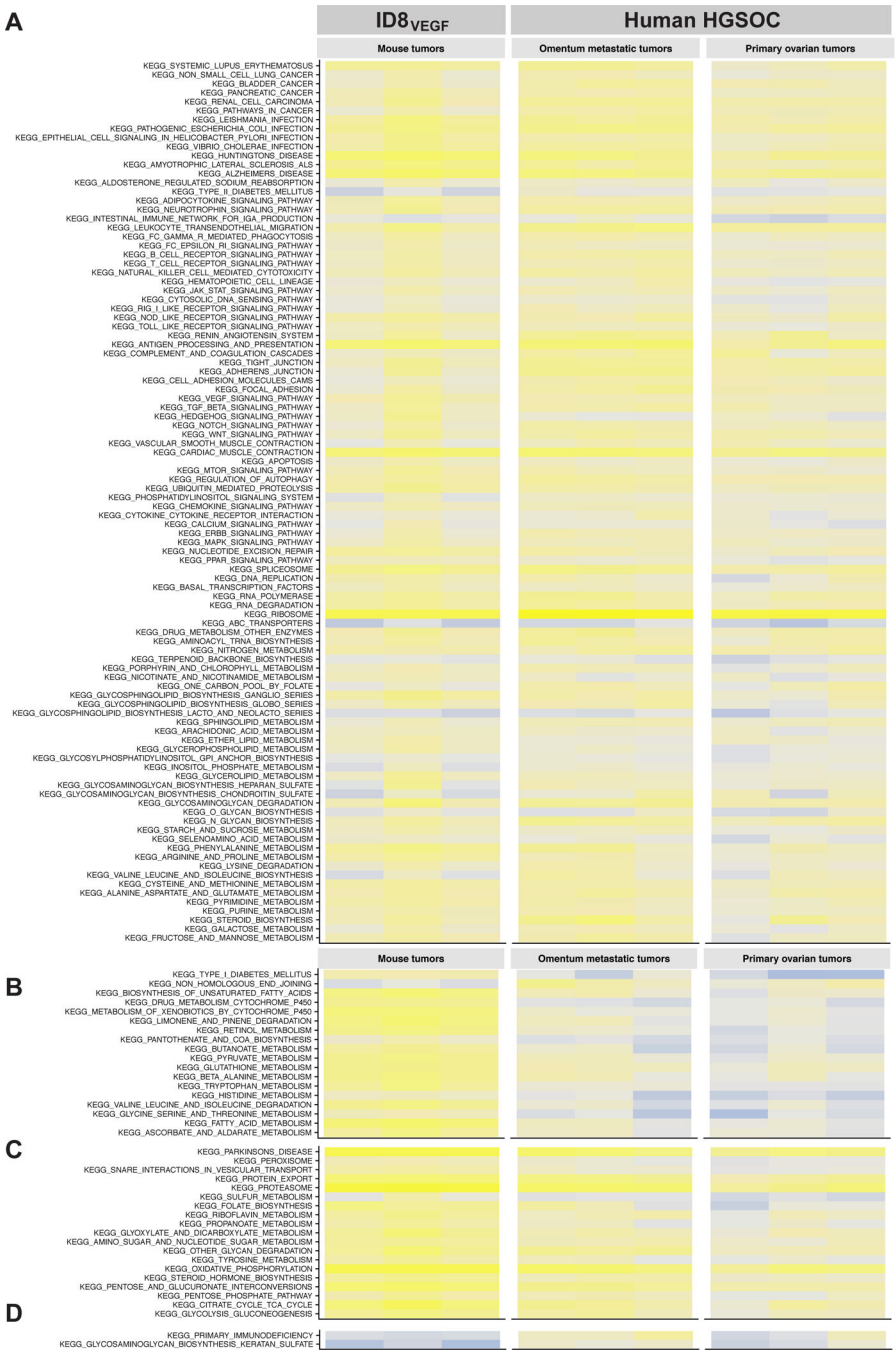

Figure 3. Deep transcriptome profiling of ID8$_{VEGF}$ and HGSOC tumors reveals very similar gene expression profiles.

A) 98 of 177 total KEGG pathways contain genes related to T-cell function. No significant expression differences were found in these genes between mouse tumor samples, human primary ovarian tumors, or human metastatic omental tumors.

B) 18 KEGG pathways revealed significant differences (FDR 1%) between mouse tumor samples and human ovarian cancer (both primary ovarian tumors and metastatic omental tumors).

C) 19 KEGG pathways revealed significant differences (FDR 1%) between mouse tumor samples and human primary ovarian tumors but not with human metastatic omental tumors. D) 2 KEGG pathways were significantly different (FDR 1%) between mouse tumor samples and human metastatic omental tumors but not with human primary ovarian tumors. No KEGG pathways were declared as significantly different between human primary ovarian tumors and human metastatic omental tumors.

A

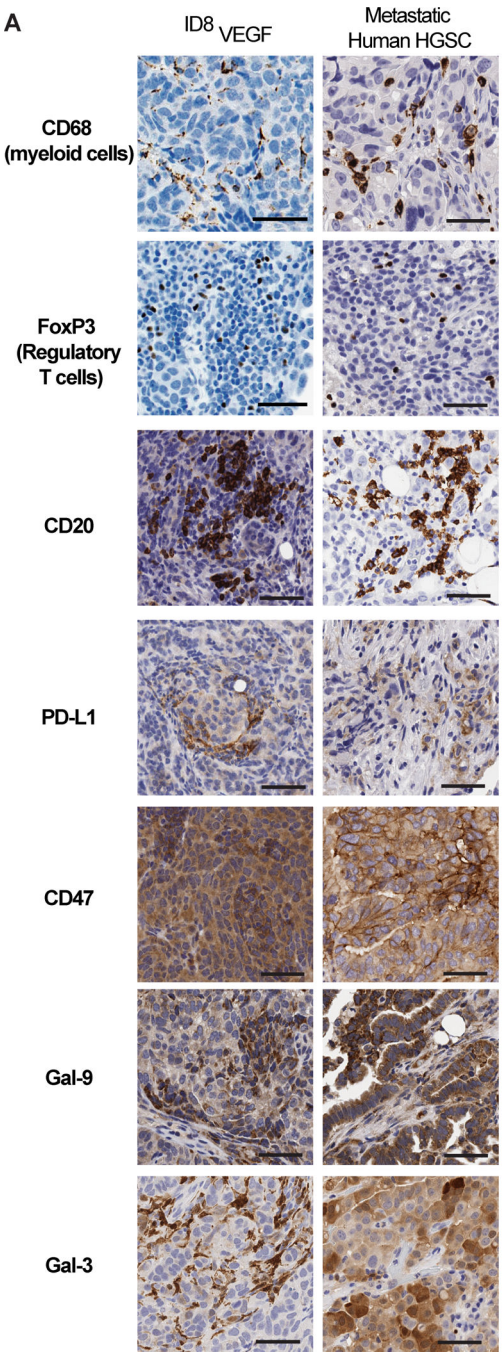

B

Sample	ID8 VEGF	Primary Tumor	Metastatic Tumor
CD68	10/10 (100%)	26/28 (92.9%)	27/28 (96.4%)
FoxP3	10/10 (100%)	3/25 (12%)	15/25 (60%)
CD20	8/8 (100%)	15/27 (55.6%)	25/28 (89.3%)
PD-L1	10/10 (100%)	25/28 (89.3%)	25/28 (89.30%)
CD47	9/9 (100%)	3/3 (100%)	3/3 (100%)
Gal-9	5/5 (100%)	3/3 (100%)	3/3 (100%)
Gal-3	7/8 (87.5%)	28/28 (100%)	27/27 (100%)

Figure 4. ID8$_{VEGF}$ tumors recapitulate immunosuppressive features of the human HGSOC TME.

A) IHC of ID8$_{VEGF}$ tumors or human metastatic HGSOC tumors for CD68, FoxP3, CD20, PD-L1, CD47, Galectin-9, or Galectin-3. IHC images are representative of 6 mice or 28 human tumor samples. Scale bar = 50 microns.

B) Proportion of samples in which positive staining for each protein was observed.

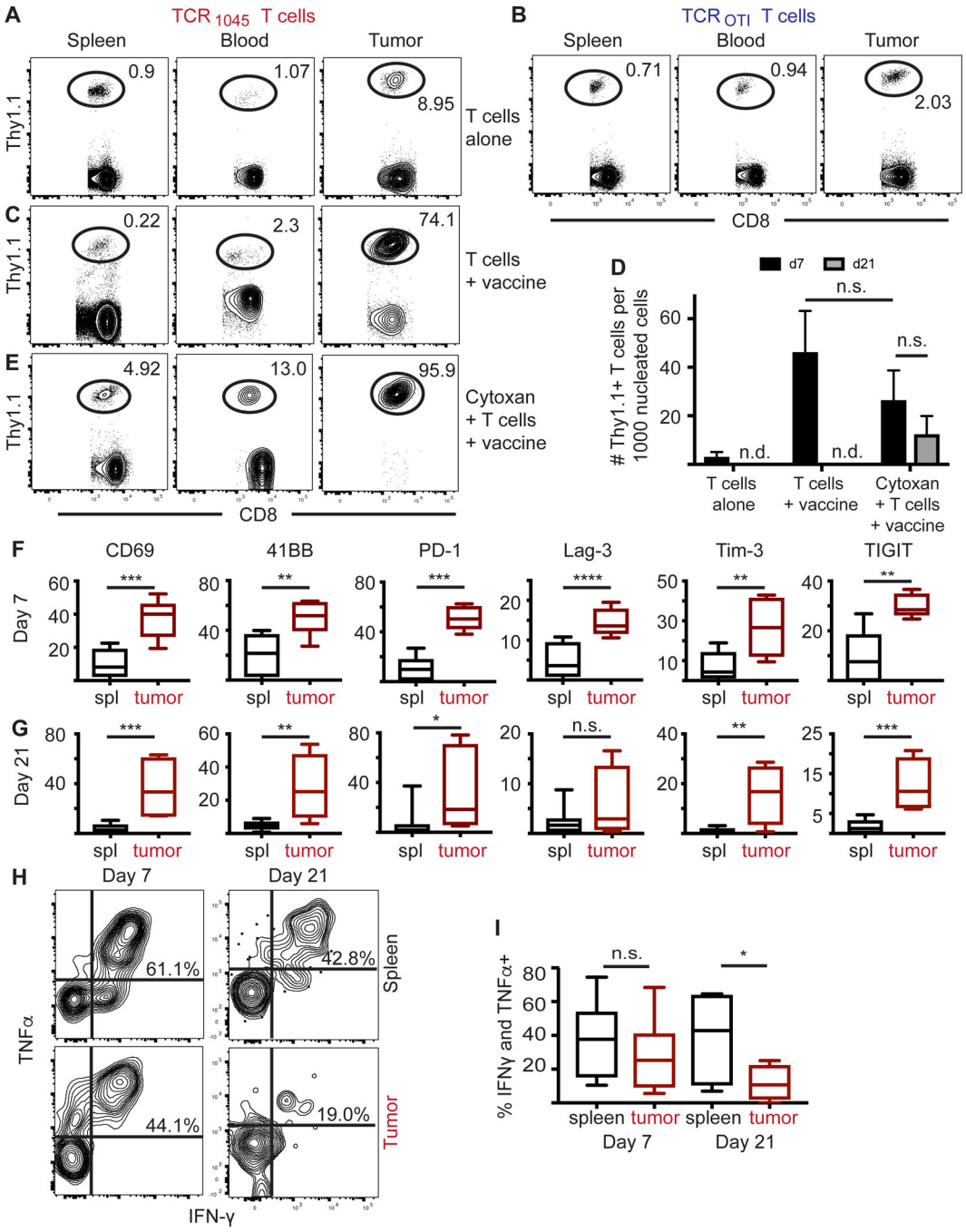

Figure 5. TCR_{1045} T cells accumulate and become dysfunctional in $ID8_{VEGF}$ tumors

Flow plots in A-C and E are representative flow plots from 2–3 independent experiments with 5–9 mice per treatment. Mice were euthanized and analyzed by flow cytometry 7 days after T-cell injection for donor T-cell infiltration ($Thy1.1^+$ in $Thy1.2^+$ host).

A, B) 1×10^7 TCR_{1045} or TCR_{OTI} $Thy1.1^+$ T cells were injected i.v. into tumor-bearing mice.

C) 1×10^7 TCR_{1045} $Thy1.1^+$ T cells were injected i.p. with peptide-pulsed irradiated splenocytes (5:1 APC:T-cell ratio). Note: for injections that include T cells and peptide-

pulsed irradiated splenocytes, mice were injected i.p. due to respiratory distress if administered i.v.

D) Quantification from all mice of donor TCR_{1045} $Thy1.1^+$ T cells in tumors 7 or 21 days after T-cell transfer. n.d. = not detectable.

E) Tumor-bearing mice received cyclophosphamide pre-treatment and, after >6-hour delay to allow for drug clearance, were injected i.p. with 1×10^7 TCR_{1045} $Thy1.1^+$ T cells and peptide-pulsed irradiated splenocytes (5:1 APC:T-cell ratio).

F, G) Frequency of TCR_{1045} T cells expressing indicated molecules, isolated from spleen (black) or tumor (red) F) 7 days or (G) 21 days after transfer. n.s. = not significant

H, I) 7 or 21 days after T-cell transfer, TCR_{1045} T cells were isolated from spleen or tumor, stimulated with Msln peptide for 5 hours *in vitro*, and evaluated for cytokine production. H) Representative flow plots or I) quantitation of double-producing $IFN\gamma^+$ $TNF\alpha^+$ $Thy1.1^+$ donor T cells isolated from spleen or tumor. Data from D, F, G, and I are aggregated from 3 independent experiments (n=3–8 mice per group). Statistical analysis performed using a student *t* test. * $p<0.05$, ** $p<0.01$, *** $p<0.001$, **** $p<0.0001$. n.s. = not significant.

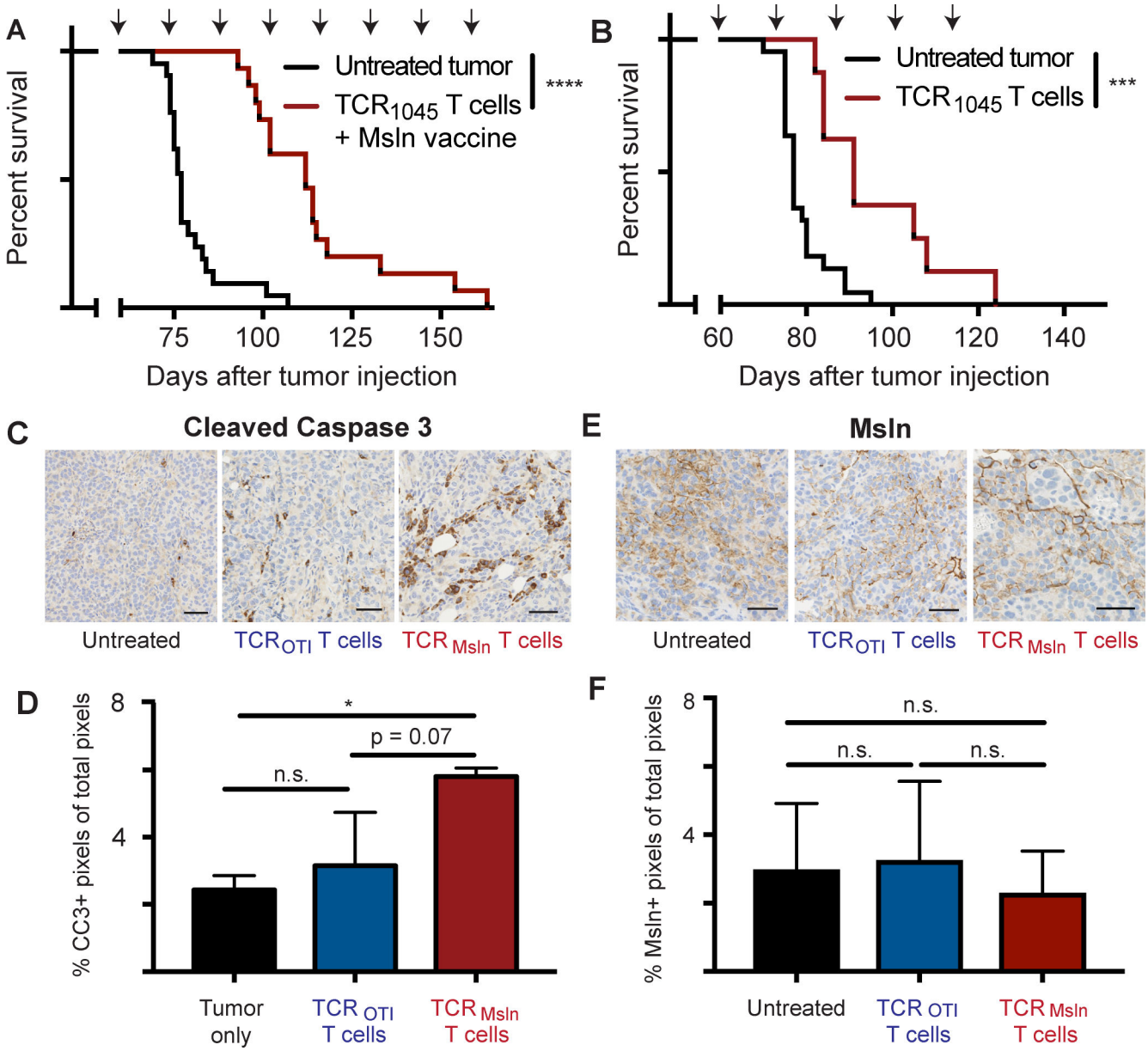

Figure 6. TCR_{1045} T cells prolong survival in $ID8_{VEGF}$ tumor-bearing mice.

A) Tumor-bearing mice received a single dose of cyclophosphamide before the 1st T-cell infusion followed by injections of 1×10^7 TCR_{1045} T cells and peptide-pulsed irradiated splenocytes (5:1 APC:T-cell ratio) i.p. every 14 days with 1×10^4 U IL2 s.c. for 10 days after each infusion. Treatment was initiated 45–52 days after tumor injection, when tumors were detectable by ultrasound. Survival data are aggregated from 4 independent experiments (n=15–21 total per group).

B) Tumor-bearing mice received 1×10^7 TCR_{1045} T cells i.v. without a vaccine every 14 days with 1×10^4 U IL2 s.c. for 10 days after each infusion. Therapy was started 45–52 days after tumor injection. Survival data was aggregated from 3 independent experiments (n=8–23 total per group). Survival curve comparison using the Log-rank (Mantel-Cox) or Gehan-Breslow-

Wilcoxon tests yielded the same statistical results. *** $p<0.0005$ **** $p < 0.0001$. Arrows above survival curves in A and B indicate the timing of T-cell infusions.

C) IHC of tumor for Cleaved Caspase 3 following 3 doses of T cells. Untreated tumor-bearing mice were euthanized at the same stage of tumor development to serve as controls.

D) Quantitation of CC3 expression by IHC from mice euthanized in panel C above.

E) IHC of tumor for Msln following 3 doses of T cells, in mice from panels C and D. Untreated tumor-bearing mice were euthanized at the same stage of tumor development to serve as controls.

F) Quantitation of Msln expression by IHC from mice euthanized in panel E above. IHC experiments are representative of 2 independent experiments (n=3 mice per group per experiment). Scale bar = 50 microns. Data are shown +/− SD. Statistical analysis performed using one-way Anova with post-hoc analysis pairwise for multiple comparisons. * $p<0.05$, n.s. = not significant

Table 1.

HLA-typing of 8 human HGSOC cell lines.

Highlighted A*02:01^{+} cell lines were used for T-cell killing assays

Cell Line	HLA A	HLA B	HLA C
Kuramochi	A*26:02:01 A*26:02:01	B*40:06:01 B*40:06:01	C*08:01:01 C*08:01:01
TYKNU	**A*02:01:01** A*26:03:01	B*15:01:01 B*35:01:01	C*03:03:01 C*07:02:01
OVKATE	A*26:01:01 A*26:01:01	B*07:02:01 B*07:02:01	C*07:02:01 C*07:02:01
OVSAHO	A*26:01:01 A*26:01:01	B*39:01:03 B*39:01:03	C*07:02:01 C*07:02:01
COV318	**A*02:01:01** A*03:01:01	B*07:02:01 B*07:02:01	C*07:02:01 C*07:02:01
OAW28	A*01:01:01 A*01:01:01	B*08:01:01 B*08:01:01	C*07:01:01 C*07:01:01
COV362	A*03:01:01 A*03:01:01	B*40:01:02 B*40:01:02	C*03:04:01 C*03:04:01
OVCAR3	**A*02:01:01** A*29:02:01	B*07:02:01 B*58:01:01	C*07:02:01 C*07:18